Polymer 50 (2009) 5945–5958

Contents lists available at ScienceDirect

Polymer

journal homepage: www.elsevier.com/locate/polymer

Synthesis, characterization, and photophysics of electroluminescent fluorene/dibenzothiophene- and fluorene/dibenzothiophene-*S*,*S*-dioxide-based main-chain copolymers bearing benzimidazole-based iridium complexes as backbones or dopants

Wei-Sheng Huang [a], Ying-Hsien Wu [b], Ying-Chan Hsu [c], Hong-Cheu Lin [a,*], Jiann T. Lin [c,**]

[a] *Department of Materials Science and Engineering, National Chiao Tung University, Hsinchu, Taiwan, ROC*
[b] *Electro-Optical Engineering and Graduate Institute of Electronics Engineering, National Taiwan University, Taipei, Taiwan, ROC*
[c] *Institute of Chemistry, Academia Sinica, Taipei, Taiwan, ROC*

ARTICLE INFO

Article history:
Received 3 August 2009
Received in revised form
29 September 2009
Accepted 3 October 2009
Available online 22 October 2009

Keywords:
Phosphorescence
Iridium complex
Charge carrier mobilities

ABSTRACT

A series of electroluminescent copolymers containing fluorene-2,8-disubstituted dibenzothiophene (**PFD**), fluorene-2,8-disubstituted dibenzothiophene-*S*,*S*-dioxide (**PFDo**) and phosphorescent benzimidazole-based iridium (Ir) complexes in the backbones were synthesized by the Suzuki coupling reaction. The thermal stabilities, HOMO/LUMO levels and triplet energy gap (E_T) values were enhanced with increasing contents of dibenzothiophene (**D**) or dibenzothiophene-*S*,*S*-dioxide (**Do**) segments in the copolymers. The relative intensities of phosphorescence and fluorescence were affected by the energy transfer and back transfer efficiencies between the polymer backbones and iridium units as evidenced by solid state PL and EL spectra. PLED devices with a configuration of ITO/PEDOT:PSS (50 nm)/metal-free copolymers (**P1**–**P5**), Ir-copolymers (**P7**–**P13**) and Ir-doped copolymers (**P3** doped with Ir-complexes **6** and **8**) (60–80 nm)/TPBI (40 nm)/LiF (1 nm)/Al (120 nm) were fabricated, and the electroluminescence (EL) efficiencies depended on the chemical constituents and triplet energies of the copolymers. The space-charge-limited current (SCLC) flow technique was used to measure the charge carrier mobilities of these copolymers, where both hole and electron mobilities were in the following order: the metal-free copolymers (**P2**, **P3** and **P5**) > Ir-doped copolymers (**P3** + 3 or 10 mol% Ir-complex **6**) > Ir-copolymers (**P7**, **P8**, **P12** and **P13**).

1. Introduction

Polymer light-emitting diodes (PLEDs) have been subjected to intensive studies for the past two decades because the spin-coating technique renders PLEDs with flexible substrates and/or large displays feasible [1]. In recent years, PLEDs based on phosphorescent iridium complexes blended in a polymer matrix have also attracted attention and highly efficient PLEDs have been achieved [2]. Nevertheless, phase separation and triplet energy confinement in such systems may lead to the aggregation of phosphors and thus induce phosphorescence quenching and reduction of the emission efficiency [3].

In order to solve those problems, PLEDs incorporating phosphorescent moieties via covalent bonds into the polymer backbones [4] or side chains [5] were developed by several research groups. In addition, it is also important to note that sufficiently large triplet energy (E_T) values were needed to suppress back energy transfer from the guest phosphors to the host polymers. For example, Park et al. designed a wide band-gap non-conjugated carbazole-based polymer (CP_0) tethered with blue-emitting FIrpic units via covalent bonds [6]. The high triplet energy ($E_T = 2.6$ eV) of CP_0 ensures a high device efficiency, with luminescence and emission efficiencies reaching 1450 cd/m^2 and 2.23 cd/A, respectively. In comparison, conjugated polymers often exhibit relatively low E_T values, such as polyfluorene (**PF**, $E_T = 2.10$ eV) [7] and polyfluorene-alt-carbazole (**P**(**F-alt-C**), $E_T = 2.18$ eV) [8]. Therefore, the covalently bonded emitters were usually used in conjunction with red-emitting iridium moieties to avoid energy back transfer [3a,5c,7a,8,9]. For a fair comparison, Holdcroft et al. developed two different iridium-based main-chain conjugated polymers [10],

* Corresponding author. Fax: +886 3 5724727.
** Corresponding author. Fax: +886 2 27831237.
E-mail addresses: linhc@cc.nctu.edu.tw (H.-C. Lin), jtlin@chem.sinica.edu.tw (J.T. Lin).

0032-3861/$ – see front matter © 2009 Elsevier Ltd. All rights reserved.
doi:10.1016/j.polymer.2009.10.011

fluorene-alt-pyridine (**PFPy**, $E_T = 2.13$ eV) and fluorene-alt-thiophene (**PFT**, $E_T = 2.88$ eV). The latter was found to have better photoluminescence (PL) and EL efficiencies because of its larger triplet energy, which could more effectively suppress the self-quenching of the phosphors.

Modification of carrier-transporting ability in polymers was also attempted. Compared with **PF**, dibenzothiophene-*S*,*S*-dioxide-fluorene co-oligomers [11] or co-polymers [12] were reported to improve electron affinity after incorporation of electron-deficient dibenzothiophene-*S*,*S*-dioxide segments. Accordingly, highly efficient blue-emitting PLEDs (external quantum efficiency (EQE) = 5.5% at 69 mA/cm^2) could be obtained by using dibenzothiophene-*S*,*S*-dioxide-fluorene co-polymers as an electron-transporting layer and poly-(9-vinylcarbazole) (PVK) as a hole-transporting layer [13]. Monkman et al. also demonstrated efficient single-layer light-emitting devices (EQE = 1.3% at 100 cd/cm^2) by using (9,9-dioctylfluorene-2,7-diyl)-dibenzothiophene-*S*,*S*-dioxide-3,7-diyl co-polymers [14].

Previously, a series of 2,8-disubstituted dibenzothiophene (**D**) [15] and 2,8-disubstituted dibenzothiophene-*S*,*S*-dioxide (**Do**) [16] derivatives containing peripheral diarylamines were developed and successfully used to fabricate efficient single-layer electroluminescent (EL) devices. Though dibenzothiophene-based [17] and dibenzothiophene-*S*,*S*-dioxide-based π-conjugating polymers [12–14] have been widely studied in PLEDs, to our knowledge, there were no reports on PLEDs using phosphor emitters. We previously developed highly phosphorescent cyclometalated iridium complexes based on benzimidazole ligands (**bi**) that could be fabricated into high performance OLEDs [18] and dendrimer-type LEDs [19]. In this article, we developed solution-processable PLED using fluorene-2,8-disubstituted dibenzothiophene (**PFD**) and fluorene-2,8-disubstituted dibenzothiophene-*S*,*S*-dioxide (**PFDo**) copolymers as the host for iridium motifs. Copolymers incorporating some phosphorescent iridium fragments into the backbones were also synthesized. Besides synthesis and characterization, the charge mobilities of the copolymers were measured by the space-charge limited current (SCLC) flow technique. PLED devices fabricated from metal-containing polymers as well as metal-free copolymers doped with standard phosphorescent iridium complexes will also be discussed.

2. Experimental

2.1. Characterization

^{1}H NMR spectra were recorded on a Bruker AMX400 spectrometer. FAB-mass spectra were collected on a JMS-700 double focusing mass spectrometer (JEOL, Tokyo, Japan) with a resolution of 3000 for low resolution and 8000 for high resolution (5% valley definition). For FAB-mass spectra, the source accelerating voltage was operated at 10 kV with a Xe gun, using 3-nitrobenzyl alcohol as a matrix. The molecular weights of polymers were determined with a Viscotek TriSEC GPC in THF solvent. The number-average and weight-average molecular weights were estimated by using a calibration curve of polystyrene standards. Elemental analyses were performed on a Perkin–Elmer 2400 CHN analyzer. Cyclic voltammetry (CV) experiments were performed with a CHI-621B electrochemical analyzer and carried out at room temperature under nitrogen at a scan rate of 100 mV/s with a conventional three-electrode configuration consisting of a platinum working electrode, an auxiliary electrode and a nonaqueous $Ag/AgNO_3$ reference electrode. The solvent used in all CV experiments was CH_2Cl_2 and the supporting electrolyte was 0.1 M tetrabutylammonium hexafluorophosphate (Bu_4NPF_6). Electronic absorption spectra were obtained on a Cary 50 Probe UV–visible spectrometer. Emission spectra were recorded in deoxygenated solutions at 298 K by a JASCO FP-6500 fluorescence spectrometer. The emission spectra in solution were collected on samples with O.D. ~0.1 at the excitation wavelength, where emission maxima were reproducible within 2 nm. The fluorescent and phosphorescent quantum yields in solutions were calculated relative to a coumarin 1 standard ($\Phi_{em} = 0.99$ in ethyl acetate) [20] and $Ir(ppy)_3$ ($\Phi_{em} = 0.40$ in toluene) [21], respectively. The quantum yields in solid films were measured with an integrating sphere under an excitation wavelength of 350 nm on a quartz glass. Phosphorescence spectra of compounds (in toluene solutions and thin films) were measured by a HORIBA Jobin-Yvon FluoroMax-P spectrometer at 77 K using a 10-ms delay time between the excitation with a microsecond flash lamp and the measurement. Luminescence quantum yields were taken as the average of three separate determinations and were reproducible within 10%. Different scanning calorimetry (DSC) measurements were carried out using a Perkin–Elmer 7 series thermal analyzer at a heating rate of 10 °C/min from 30 to 300 °C. Thermogravimetric analysis (TGA) measurements were performed on a Perkin Elmer Pyris 1 TGA at a heating rate of 10 °C/min under nitrogen.

2.2. Light-emitting diode (LED) device fabrication

Prepatterned ITO substrates with an effective individual device area of 3.14 mm^2 were cleaned via repeated ultrasonic washing with detergent, deionized water, ethanol and finally oxygen plasma treatment. A layer of poly(ethylenedioxythiophene):poly(styrene–sulfonic acid) (PEDOT:PSS) (Baytron AI4083) with a thickness of 50 nm was spin-coated on the pre-cleaned ITO glass substrates as a hole injection layer and then baked at 100 °C in air for 1 h. Then, the polymers were dissolved in dichlorobenzene (concentration: 10 mg mL^{-1} for the polymers) and filtered with a 0.2 μm filter. A thin film of polymer was coated at a spin rate of 1500 rpm (revolution per min.). The film thickness of the polymer layer was around 60–80 nm, measured by a surface profilometer Dektak 3 (Veeco/Sloan Instrument Inc.). Afterward, a layer (with a thickness of 40 nm) of electron transporting 1,3,5-tris(*N*-phenylbenzimidazol-2-yl)benzene (TPBI) was deposited under vacuum. Finally, a layer of LiF/Al (1 nm/120 nm) was thermally evaporated as a cathode in a vacuum chamber (under a pressure of less than 2.5×10^{-5} Torr). *I–V* curves were measured on a Keithley 2400 Source Meter in ambient environment, and the light intensity was measured with a Newport 1835 Optical Meter.

2.3. Hole-only and electron-only device fabrication

The hole-only and electron-only devices in this study consist of polymer films sandwiched between transparent ITO anodes and cathodes, where the device fabrication was the same as that for PLEDs. In the hole-only device, the modified ITO surface was obtained by spin-coating a layer of poly(ethylene dioxythiophene): polystyrenesulfonate (PEDOT:PSS) (~50 nm). After baking at 100 °C for 1 h, the substrates were then transferred into a nitrogen-filled glove box. The active layer was spin-coated (spin rate = 1000 rpm; spin time = 40 s) on top of PEDOT:PSS and then dried in covered glass Petri dishes. Subsequently, 10 and 120 nm thicknesses of MoO_3 and aluminum were thermally evaporated, respectively, through a shadow mask. In the electron-only device, the PEDOT:PSS layer was replaced with Cs_2CO_3, which has been used as an efficient electron injection layer. The modified ITO surface was obtained by spin-coating a layer of Cs_2CO_3 (~2 nm). The active layer was spin-coated (spin rate = 1000 rpm; spin time = 40 s) on top of the Cs_2CO_3 and then dried in covered glass Petri dishes. Consequently, 40 and 70 nm thicknesses of Ca and aluminum were thermally evaporated, respectively.

2.4. Materials

Chemicals and solvents were reagent grades and purchased from Aldrich, Acros, TCI, and Lancaster Chemical Co. Solvents were dried by standard procedures. All reactions and manipulations were carried out under N_2 with the use of standard inert atmosphere and Schlenk techniques. All column chromatography experiments were performed by using silica gel (230–400 mesh, Macherey-Nagel GmbH & Co.) as the stationary phase in a column which is 25–35 cm in length and 2.5 cm in diameter.

2.4.1. 2-(4-Bromophenyl)-1-phenyl-1H-benzimidazole (**1**) (pbi-Br)

N-Phenyl-*o*-phenylenediamine (1 equiv) and 4-bromobenzaldehyde (1 equiv.) were dissolved in 50 mL of 2-methoxyethanol. The mixture was refluxed for 48 h under nitrogen. The volatiles were removed under vacuum and the resulting solid was extracted by dichloromethane. The organic extract was washed with brine solution and dried over anhydrous $MgSO_4$, and then it was filtered and evaporated to dryness. The crude product was purified by column chromatography (silica gel) using a mixture of dichloromethane and hexanes (1:1 by volume) as the eluent. The pure compound was acquired as a white solid with a 60% yield. ^{1}H NMR ($CDCl_3$, 400 MHz, ppm): δ 7.68 (d, $J = 8.0$ Hz, 1H), 7.35–7.29 (m, 4H), 7.24–7.20 (m, 1H), 7.15–7.02 (m, 7H). FABMS: m/z 348.9 $(M)^+$. Anal. calcd. for $C_{19}H_{13}BrN_2$: C, 65.35; H, 3.75; N, 8.02. Found: C, 65.22; H, 3.78; N, 8.01.

2.4.2. 2-(4-(9,9-Dihexyl-9H-fluoren-2-yl)phenyl)-1-phenyl-1H-benzimidazole (**2**) (pbiF)

To a mixture of toluene and aqueous solution of K_2CO_3 (1:1 v/v, 40 mL), compound **1** (1.39 g, 4.0 mmol), 2-(4,4,5,5-tetramethyl-1,3,2-dioxaborolan-2-yl)-9,9-dioctylfluorene (1.73 g, 4.0 mmol), and tetrakis(triphenylphosphine)palladium (100 mg, 0.040 mmol) were added to react for 24 h. After cooling, the reaction was quenched with water and the mixture was extracted with dichloromethane. The combined extract was then washed with brine, dried over $MgSO_4$, and evaporated to dryness. The crude product was isolated by column chromatography on a silica gel column using a mixture of dichloromethane and hexanes (1:4 by volume) as the eluent. The pure compound was obtained as a bright yellow powder with a 40% yield (1.06 g). ^{1}H NMR ($CDCl_3$, 400 MHz, ppm): δ 8.19 (s, 1H), 7.92 (d, $J = 8.0$ Hz, 1H), 7.74 (d, $J = 8.0$ Hz, 2H), 7.70 (d, $J = 8.4$ Hz, 2H), 7.62 (d, $J = 8.4$ Hz, 2H), 7.58–7.53 (m, 4H), 7.41–7.27 (m, 8H), 2.01–1.97 (m, 4H), 1.13–1.03 (m, 20H), 0.75 (t, $J = 7.5$ Hz, 6H), 0.66–0.63 (m, 4H). FABMS: m/z 659.2 $(M + H)^+$. Anal. calcd. for $C_{44}H_{46}N_2$: C, 87.66; H, 7.69; N, 4.65. Found: C, 87.42; H, 7.78; N, 4.41.

2.4.3. 2-(4-(4-Bromobenzyloxy)phenyl)-1-phenyl-1H-benzimidazole (**3**) (pbiOPh-Br)

2-(Phenol-4yl)-1-phenyl-1*H*-benzimidazole [19] (1.66 g, 5.8 mmol), K_2CO_3 (1.0 g, 5.88 mmol), and 4-bromobenzylbromide (1.45 g, 5.88 mmol) were dissolved in 30 mL of *N*,*N*-dimethylformamide (DMF). The mixture was heated to react at 100 °C for 24 h. After cooling, the reaction was quenched with water and the mixture was extracted with dichloromethane. The combined extract was then washed with brine, dried over $MgSO_4$, and evaporated to dryness. The crude product was isolated by column chromatography on a silica gel column using a mixture of dichloromethane and hexanes (1:4 by volume) as the eluent. The pure compound was a white solid with a 73% yield. ^{1}H NMR ($CDCl_3$, 300 MHz, ppm): δ 7.88 (d, $J = 7.8$ Hz, 1H), 7.54–7.46 (m, 7H), 7.35–7.21 (m, 7H), 6.86 (d, $J = 7.8$ Hz, 2H), 4.97 (s, 2H). FABMS: m/z 455.1 $(M + H)^+$. Anal. calcd. for $C_{26}H_{19}BrN_2O$: C, 68.58; H, 4,21; N, 6.15. Found: C, 68.32; H, 4.18; N, 6.21.

2.4.4. 2-(4-(4-(9,9-Dihexyl-9H-fluoren-2-yl)benzyloxy)phenyl)-1-phenyl-1H-benzimidazole (**4**) (pbiOPhF)

Compound **4** was synthesized by the same procedure as illustrated for compound **3** except that 4-bromobenzylbromide was used instead of 2-(4-(bromomethyl)phenyl)-9,9-dihexyl-9*H*-fluorene. White solid. Yield = 56%. ^{1}H NMR ($CDCl_3$, 400 MHz, ppm): δ 7.84 (d, $J = 8.0$ Hz, 1H), 7.72 (d, $J = 8.0$ Hz, 1H), 7.69 (d, $J = 7.2$ Hz, 1H), 7.65 (d, $J = 8.0$ Hz, 2H), 7.55–7.45 (m, 9H), 7.31–7.28 (m, 6H), 7.22–7.18 (m, 2H), 6.91 (d, $J = 8.8$ Hz, 2H), 5.09 (s, 2H, OCH_2), 1.99–1.96 (m, 4H, CH_2), 1.09–1.01 (m, 12H, CH_2), 0.73 (t, $J = 6.8$ Hz, 6H, CH_3), 0.66–0.64 (m, 4H, CH_2). FABMS: m/z 709.5 $(M + H)^+$. Anal. Calcd. for $C_{51}H_{52}N_2O$: C, 86.40; H, 7.39; N, 3.95. Found: C, 86.54; H, 7.40; N, 3.67.

2.4.5. $(pbi\text{-}Br)_2Ir(acac)$ (**5**)

To a flask containing $IrCl_3 \cdot nH_2O$ (176 mg, 0.5 mmol) and compound **1** (700 mg, 2.0 equiv.), a mixture of 2-methoxyethanol (S) and water (3:1 v/v, 25 mL) was added. The mixture was then refluxed to react for 48 h and cooled to room temperature. After cooling, the reaction was quenched with water, extracted with dichloromethane, and dried under vacuum. The solids yielded were collected by filtration and evaporation to give the crude product. The crude product, i.e., μ-chloro-bridged Ir(III) dimmer, was mixed with Na_2CO_3 (0.30 g, 3.0 mmol), 2,4-pentanedione (0.30 g, 3.0 mmol), and 2-methoxyethanol (20 mL) in a flask. The mixture was heated to react for 24 h. After cooling, the reaction was quenched with water and the mixture was extracted with dichloromethane. The combined extracts were then washed with brine, dried over $MgSO_4$, and evaporated to dryness. The crude product was isolated by column chromatography on a silica gel column using a mixture of CH_2Cl_2 and *n*-hexanes (1:1 by volume) as the eluent to afford the pure compound as a yellow solid with a 65% yield. ^{1}H NMR ($CDCl_3$, 400 MHz, ppm): δ 7.68–7.63 (m, 8H), 7.60–7.58 (m, 4H), 7.32–7.27 (m, 4H), 7.14–7.11 (m, 2H), 6.64 (dd, $J = 8.0$ and $J = 2.0$ Hz, 2H), 6.49 (d, $J = 2.0$ Hz, 2H), 6.38 (d, $J = 8.4$ Hz, 2H), 5.25 (s, 1H), 1.84 (s, 6H). FABMS: m/z 986.0 $(M)^+$. Anal. calcd. for $C_{43}H_{31}Br_2IrN_4O_2$: C, 52.29; H, 3.16; N, 5.67. Found: C, 52.55; H, 3.26; N, 5.56.

2.4.6. $(pbiF)_2Ir(acac)$ (**6**)

Compound **6** was synthesized by the same procedure as illustrated for compound **5** except that compound **2** was used instead of compound **1**. The product was isolated as an orange solid with a 40% yield. ^{1}H NMR ($CDCl_3$, 400 MHz, ppm): δ 7.87 (s, 2H), 7.88 (dd, $J = 7.2$ and 1.6 Hz, 2H), 7.69–7.55 (m, 10H), 7.50–7.48 (m, 2H), 7.46 (d, $J = 8.0$ Hz, 2H), 7.37–7.34 (m, 4H), 7.24–7.15 (m, 8H), 7.01 (s, 2H), 6.82 (s, 2H), 6.80 (dd, $J = 8.0$ and 1.6 Hz, 2H), 6.60 (d, $J = 8.0$ Hz, 2H), 5.29 (s, 1H), 1.91 (s, 6H), 1.90–1.58 (m, 8H), 1.13–1.03 (m, 24H), 0.75 (t, $J = 7.6$ Hz, 12H), 0.66–0.63 (m, 8H). FABMS: m/z 1495.8 $(M)^+$. Anal. calcd. for $C_{93}H_{97}IrN_4O_2$: C, 74.71; H, 6.54; N, 3.75. Found: C, 74.24; H, 6.75; N, 3.42.

2.4.7. $(pbiOPh\text{-}Br)_2Ir(acac)$ (**7**)

Compound **7** was synthesized by the same procedure as illustrated for compound **5** except that compound **3** was used instead of compound **1**. The product was isolated as an orange solid with a 40% yield. ^{1}H NMR ($CDCl_3$, 400 MHz, ppm): δ 7.70–7.60 (m, 8H), 7.46–7.41 (m, 2H), 7.27–7.18 (m, 10H), 7.10–7.05 (m, 4H), 6.86 (d, $J = 8.0$ Hz, 2H), 6.46–6.44 (m, 2H), 6.12–6.02 (m, 4H), 5.21 (s, 1H), 4.57–4.54 (m, 4H), 1.83 (s, 6H). FABMS: m/z 1200 $(M)^+$. Anal. calcd. for $C_{57}H_{43}Br_2IrN_4O_4$: C, 74.71; H, 6.54; N, 3.75. Found: C, 74.52; H, 6.35; N, 3.71.

2.4.8. $(pbiOPhF)_2Ir(acac)$ (**8**)

Compound **8** was synthesized by the same procedure as illustrated for compound **5** except that compound **4** was used instead of

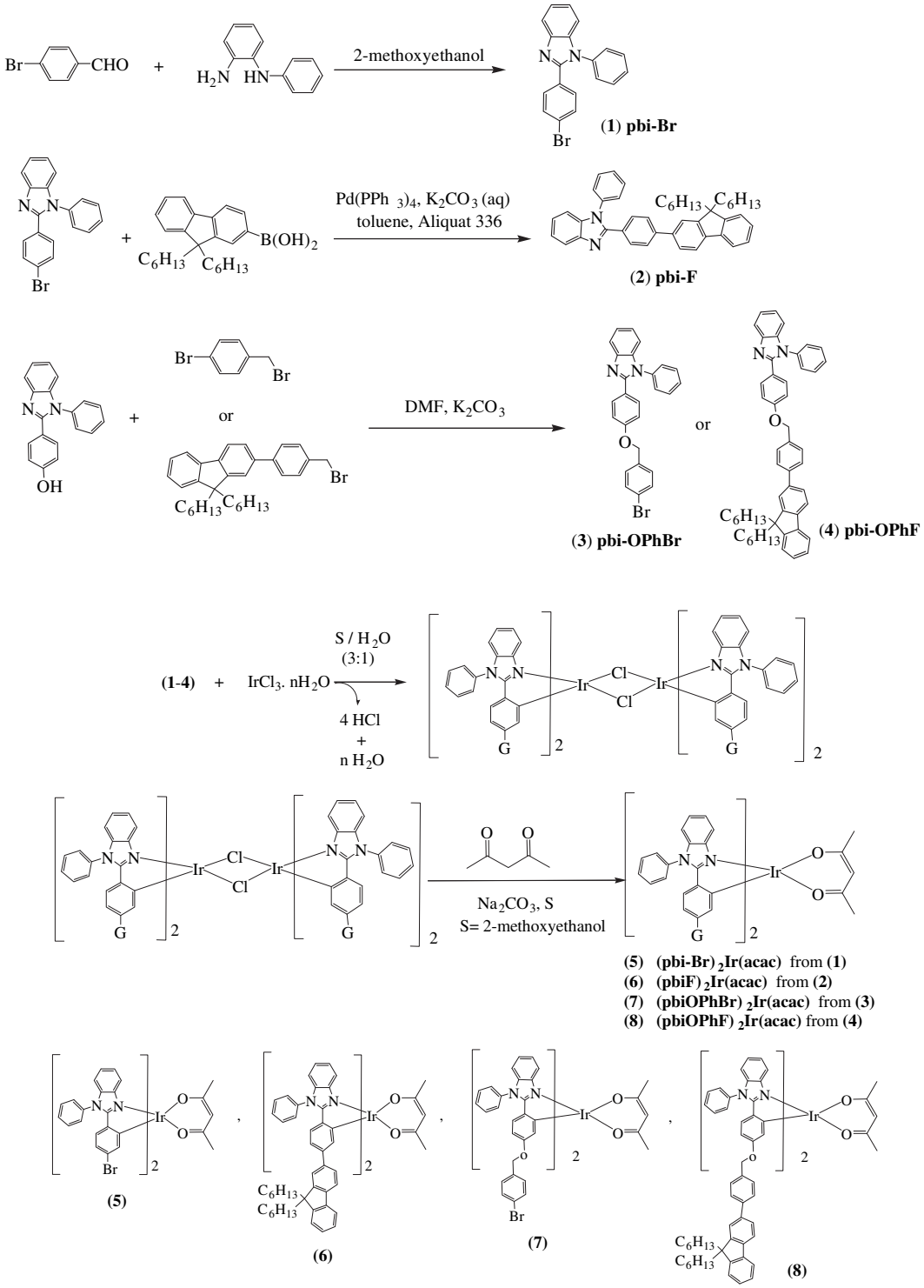

Scheme 1. Synthesis of benzimidazole ligands **1**–**4** and Ir-complexes **5**–**8**.

compound **1**. The product was isolated as an orange solid with a 42% yield. ^{1}H NMR ($CDCl_3$, 400 MHz, ppm): δ 7.73–7.69 (m, 6H), 7.63–7.56 (m, 6H), 7.50–7.45 (m, 14H), 7.30–7.28 (m, 8H), 7.13 (d, J = 7.6 Hz, 4H), 7.07 (d, J = 7.6 Hz, 2H), 6.49 (d, J = 8.8 Hz, 2H), 6.15 (dd, J = 8.8 and 1.6 Hz, 2H), 6.12 (d, J = 1.6 Hz, 2H), 5.23 (s, 1H), 4.65–4.62 (m, 4H), 1.96–1.90 (m, 8H), 1.84 (s, 6H), 1.17–1.01 (m, 24H), 0.74–0.70 (m, 12H), 0.70–0.63 (m, 8H). FABMS: m/z 1706.8 $(M)^+$. Anal. calcd. for $C_{107}H_{109}IrN_4O_4$: C, 75.28; H, 6.44; N, 3.28. Found: C, 75.72; H, 6.57; N, 3.06.

2.4.9. General procedure of copolymerization by Suzuki cross-coupling method

The following generalized procedure was used for the preparation of all copolymers. To a 50 mL two-necked flask charged with a condenser, tricaprylymethylammonium chloride (Aliquat 336) ($\sim$20 wt% based on the monomer), dibromide (compounds **5** or **7**, **9** or **10**, and **11**, 1 equiv.), diboronate (compound **12**, 1 equiv.), and $Pd(PPh_3)_4$ (0.005 equiv) were added. After the flask was evacuated and refilled with nitrogen for three times, toluene

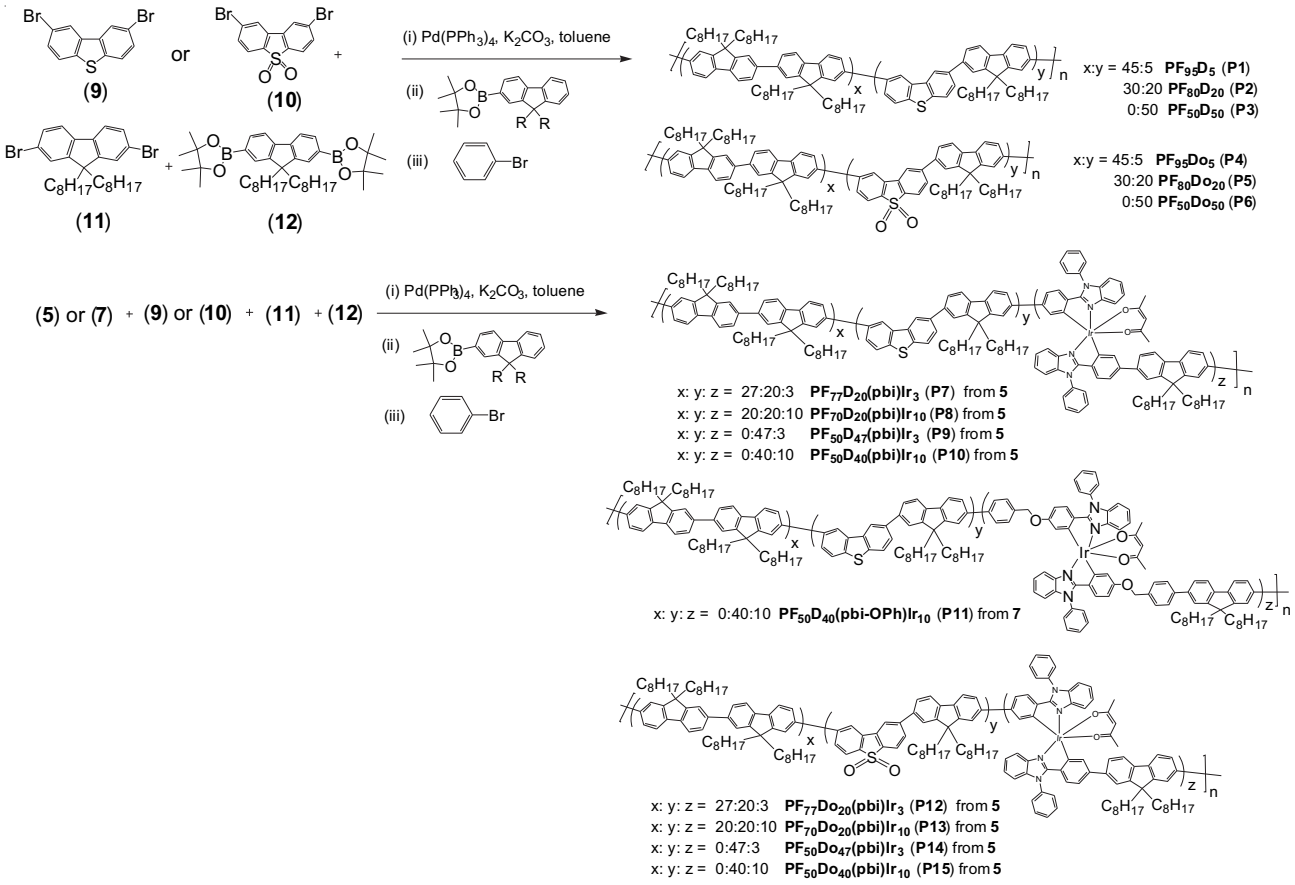

Scheme 2. Synthetic routes of copolymers **P1**–**P15**.

(1.0 mL) was added. Once all the monomers were dissolved, an aqueous solution of K_2CO_3 (2 M, 1.0 mL) was added. The mixture was heated to react at 100 °C and stirred for 48 h under nitrogen. 2-(4,4,5,5-Tetramethyl-1,3,2-dioxaborolan-2-yl)-9,9-dioctyl-fluorene (100 mg) was added and stirred at the same temperature for 12 h. Then, bromobenzene (0.5 mL) was added to the solution to react for another 12 h. The mixture was cooled and poured into a mixture of methanol and water (100 mL, 2:1 v/v). The crude copolymer was filtered and washed with excess methanol, water, and acetone, and then evaporated to dryness. The polymer was dissolved in dichloromethane and precipitated in methanol for two times. Except for **P6**, **P14**, and **P15**, the product was further purified by flash chromatography using silica gel and eluted with a mixture of dichloromethane and THF (3:1 v/v) as the eluent. A general nomenclature for the copolymers (**P1**–**P15**) with respect to abbreviations of their monomers and their mol% were adopted. For example, **$PF_{70}D_{20}$(pbi)Ir_{10}** (**P8**) was synthesized from the composition of the following monomers: 10 mol% of Ir-complex **5**, 20 mol% of 2,8-dibromo-dibenzothiophene (**9**) and 70 mol% of fluorenes (note: both **11** and **12** will contribute to the fluorene unit, **F**, in the polymer). In addition, **$PF_{77}Do_{20}$(pbi)Ir_3** (**P12**) was synthesized from the composition of the following monomers: 3 mol% Ir-complex **5**, 20 mol% of 2,8-dibromo-dibenzothiophene-*S*,*S*-dioxide (**10**) and 77 mol% of **F**, respectively.

$PF_{95}D_5$ (**P1**): Light-green solid. Yield = 60%. Anal. calcd for $(C_{29}H_{40})_{95}(C_{12}H_6S)_5$: C, 89.38; H, 10.20. Found: C, 88.78; H, 9.86. Weight-average molecular weight (M_w): 20,700 Da. PDI = 1.95.

$PF_{80}D_{20}$ (**P2**): Light-green solid. Yield = 58%. Anal. calcd for $(C_{29}H_{40})_{80}(C_{12}H_6S)_{20}$: C, 88.53; H, 9.63. Found: C, 87.63; H, 9.04. Weight-average molecular weight (M_w): 8000 Da. PDI = 1.33.

$PF_{50}D_{50}$ (**P3**): Light-green solid. Yield = 43%. ^{1}H NMR ($CDCl_3$, 400 MHz, ppm): δ 8.54 (s, dibenzothiophene ring), 7.97 (d, J = 8.8 Hz, dibenzothiophene ring), 7.90–7.77 (m, dibenzothiophene and fluorine ring), 7.69–7.60 (m, fluorine ring), 2.12 (br, –CH_2), 1.15–1.00 (m, CH_2), 0.90–0.75 (m, CH_2 and CH_3). Anal. calcd for $(C_{29}H_{40})_{50}(C_{12}H_6S)_{50}$: C, 86.27; H, 8.11. Found: C, 85.77; H, 7.98. Weight-average molecular weight (M_w): 7380 Da. DPI = 1.47.

$PF_{95}Do_5$ (**P4**): Gray solid. Yield = 70%. Anal. calcd for $(C_{29}H_{40})_{95}(C_{12}H_6O_2S)_5$: C, 89.00; H, 10.15. Found: C, 88.24; H, 9.73. Weight-average molecular weight (M_w): 49,000 Da. PDI = 1.85.

$PF_{80}Do_{20}$ (**P5**): Gray solid. Yield = 55%. Anal. calcd for $(C_{29}H_{40})_{80}(C_{12}H_6O_2S)_{20}$: C, 86.93; H, 9.45. Found: C, 86.34; H, 9.03. Weight-average molecular weight (M_w): 19,600 Da. PDI = 1.86.

$PF_{50}Do_{50}$ (**P6**): Gray solid. Yield = 30%. ^{1}H NMR ($CDCl_3$, 400 MHz, ppm): δ 8.17–8.10 (m, dibenzothiophene-*S*,*S*-dioxide ring), 7.96–7.87 (m, dibenzothiophene-*S*,*S*-dioxide ring), 7.84–7.81 (m, dibenzothiophene-*S*,*S*-dioxide and fluorine ring), 7.69–7.60 (m,fluorine ring), 2.12 (br, β–CH_2), 1.15–1.00 (m, CH_2), 0.90–0.75 (m, CH_2 and CH_3). Anal. calcd for $(C_{29}H_{40})_{50}(C_{12}H_6O_2S)_{50}$: C, 81.69; H, 7.68. Found: C, 80.78; H, 7.56. Weight-average molecular weight (M_w): 5310 Da. PDI = 1.32.

$PF_{77}D_{20}$(pbi)Ir_3 (**P7**): Brown solid. Yield = 60%. Anal. calcd for $(C_{29}H_{40})_{77}$ $(C_{12}H_6S)_{20}(C_{43}H_{31}IrN_4O_2)_3$: C, 86.69; H, 9.20; N, 0.47. Found: C, 87.59; H, 9.13; N, 0.39. Weight-average molecular weight (M_w): 20,900 Da. PDI = 1.83.

$PF_{70}D_{20}$(pbi)Ir_{10} (**P8**): Yellow-orange solid. Yield = 55%. Anal. calcd for $(C_{29}H_{40})_{70}(C_{12}H_6S)_{20}(C_{43}H_{31}IrN_4O_2)_{10}$: C, 82.88; H, 8.32; N, 1.43. Found: C, 82.59; H, 8.49 N, 1.59. A weight-average molecular weight (M_w): 9110 Da. PDI = 1.61.

$PF_{50}D_{47}$(pbi)Ir_3 (**P9**): Orange solid. Yield = 55%. Anal. calcd for $(C_{29}H_{40})_{50}(C_{12}H_6S)_{47}(C_{43}H_{31}IrN_4O_2)_3$: C, 84.45; H, 7.85; N, 0.55.

Found: C, 83.24; H, 7.48; N, 0.43. Weight-average molecular weight (M_w): 20,900 Da. PDI = 1.83.

$PF_{50}D_{40}$(pbi)Ir_{10} (**P10**): Orange solid. Yield = 45%. ^{1}H NMR ($CDCl_3$, 400 MHz, ppm): δ 8.54 (s, dibenzothiophene ring), 7.97 (d, J = 8.8 Hz, dibenzothiophene ring), 7.90–7.77 (m, dibenzothiophene and fluorine ring), 7.69–7.60 (m, fluorine ring), 2.12 (br, β–CH_2), 1.15–1.00 (m, CH_2), 0.90–0.75 (m, CH_2 and CH_3). Anal. calcd for $(C_{29}H_{40})_{50}(C_{12}H_6S)_{40}(C_{43}H_{31}IrN_4O_2)_{10}$: C, 80.99; H, 7.34; N, 1.60. Found: C, 80.59; H, 7.49; N, 1.59. Weight-average molecular weight (M_w): 8000 Da. PDI = 1.33.

$PF_{50}D_{40}$(pbiOPh)Ir_{10} (**P11**): Yellow solid. Yield = 55%. ^{1}H NMR ($CDCl_3$, 400 MHz, ppm): δ 8.54 (s, dibenzothiophene ring), 7.97 (d, J = 8.8 Hz, dibenzothiophene ring), 7.90–7.77 (m, dibenzothiophene and fluorine ring), 7.69–7.60 (m, fluorine ring), 2.12 (br, β–CH_2), 1.15–1.00 (m, CH_2), 0.90–0.75 (m, CH_2 and CH_3). Anal. calcd for $(C_{29}H_{40})_{50}(C_{12}H_6S)_{40}(C_{57}H_{41}IrN_4O_4)_{10}$: C, 80.93; H, 7.20; N, 3.46. Found: C, 79.59; H, 7.49; N, 3.14. Weight-average molecular weight (M_w): 10,500 Da. PDI = 1.42.

$PF_{77}Do_{20}$(pbi)Ir_3 (**P12**): Brown solid. Yield = 55%. Anal. calcd for $(C_{29}H_{40})_{77}(C_{12}H_6SO_2)_{20}(C_{43}H_{31}IrN_4O_2)_3$: C, 85.17; H, 9.05; N, 0.46. Found: C, 85.71; H, 8.60; N, 0.39. Weight-average molecular weight (M_w): 16,700 Da. PDI = 1.63.

$PF_{70}Do_{20}$(pbi)Ir_{10} (**P13**): Brown solid. Yield = 63%. Anal. calcd for $(C_{29}H_{40})_{70}(C_{12}H_6SO_2)_{20}(C_{43}H_{31}IrN_4O_2)_{10}$: C, 81.54; H, 8.19; N, 1.41. Found: C, 82.06; H, 8.16; N, 1.29. Weight-average molecular weight (M_w): 17400 Da. PDI = 1.65.

$PF_{50}Do_{47}$(pbi)Ir_3 (**P14**): Orange solid. Yield = 45%. Anal. calcd for $(C_{29}H_{40})_{50}(C_{12}H_6SO_2)_{47}(C_{43}H_{31}IrN_4O_2)_3$: C, 80.48; H, 7.48; N, 0.53. Found: C, 79.77; H,7.24; N 0.34. Weight-average molecular weight (M_w): 5600 Da. PDI = 1.51.

$PF_{50}Do_{40}$(pbi)Ir_{10} (**P15**): Orange solid. Yield = 43%. ^{1}H NMR ($CDCl_3$, 400 MHz, ppm): δ 8.17–8.10 (m, dibenzothiophene-*S*,*S*-dioxide ring), 7.96–7.87 (m, dibenzothiophene-*S*,*S*-dioxide ring), 7.84–7.81 (m, dibenzothiophene-*S*,*S*-dioxide and fluorine ring), 7.69–7.60 (m, fluorine ring), 2.12 (br, β–CH_2), 1.15–1.00 (m, CH_2), 0.90–0.75 (m, CH_2 and CH_3). Anal. calcd for $(C_{29}H_{40})_{50}(C_{12}H_6SO_2)_{40}(C_{43}H_{31}IrN_4O_2)_{10}$: C, 78.13; H, 7.08; N, 1.54. Found: C, 77.52; H, 6.78; N, 1.34. Weight-average molecular weight (M_w): 3690 Da. PDI = 1.51.

3. Results and discussion

3.1. Synthesis and characterization

The synthetic routes and chemical structures of the copolymers are shown in Schemes 1 and 2. The benzimidazole ligands **1**–**4** and Ir-complexes **5**–**8** were synthesized following the same or similar literature procedures [18,19]. The 2,8-dibromo-dibenzothiophene (compound **9**) and 2,8-dibromo-dibenzothiophene-*S*,*S*-dioxide (compound **10**) were synthesized by following published methods [22]. Copolymerization of dibromo-substituted Ir-complex **5** or **7**, compound **9** or **10**, and fluorenes (compounds **11** and **12**) was achieved via the Suzuki coupling reaction. For systematic studies of the device performance and the optical properties of these copolymers, the feed ratios of iridium units were controlled at the levels of 3 and 10 mol%, and compound **9** (or **10**) at the levels of 5, 20 and 50 mol%, respectively. Except for copolymers with high **Do** contents (**P6**, **P14**, and **P15**), all copolymers and Ir-complexes exhibit good solubilities in dichloromethane (CH_2Cl_2) and tetrahydrofuran (THF). All copolymers were characterized by ^{1}H NMR spectroscopy, gel permeation chromatography (GPC) and elemental analyses. The actual compositions of the copolymers and the feed ratios of the monomers are listed in Table 1. The weight-average molecular weights (M_n) of these copolymers lie in the range of 3690–26,400 g/mol with polydispersity index (PDI) values ranging from 1.32 to 1.95.

Table 1
Molecular weight data of copolymers **P1**–**P15**.

Copolymer	M_n[a] (g mol^{-1})	M_w[a] (g mol^{-1})	PDI (M_w/M_n)	F:D (or Do):Ir complexes (molar ratio)[b]	
				Co-monomer in feed ratio	Composition in copolymer
P1	10600	20700	1.95	95:5:0	94:6:0
P2	16400	28000	1.70	80:20:0	83:17:0
P3	6030	8560	1.42	50:50:0	53:47:0
P4	26400	49000	1.85	95:5:0	97:3:0
P5	10500	19600	1.86	80:20:0	88:12:0
P6	4000	5310	1.32	50:50:0	51:49:0
P7	11400	20900	1.83	77:20:3	77.5:19.5:3
P8	5650	9110	1.61	70:20:10	72:18.7:9.3
P9	6000	8000	1.33	50:47:3	49.5:48.2:2.3
P10	5000	7380	1.47	50:40:10	52.2:38.5:9.3
P11	7400	10500	1.42	50:40:10	56.4:35:8.6
P12	10200	16700	1.63	77:20:3	80:18.2:1.8
P13	10500	17400	1.65	70:20:10	71.8:20:8.2
P14	3700	5600	1.51	50:47:3	51.5:46.5:2
P15	2440	3690	1.51	50:40:10	53:37.5:9.5

[a] Molecular weights were determined by GPC using polystyrene standards.
[b] The iridium contents in copolymers were estimated by ^{1}H NMR.

3.2. Thermal analysis

The thermal properties of all copolymers were investigated by differential scanning calorimetry (DSC) and thermal gravimetric analysis (TGA) under nitrogen. Thermal analysis data for the copolymers and Ir-complexes are given in Table 2. All copolymers (**P1**–**P15**) exhibited good thermal stabilities with thermal decomposition temperatures (T_d at 5% weight loss) ranging from 357 to 442 °C. The T_d value decreases as the iridium feed ratio increases, indicating that covalently bonded iridium segments in polymer backbones decrease the thermal stability of the polymers. The glass

Table 2
Electrochemical and thermal properties of Ir-complexes **5**–**8** and Ir-copolymers **P1**–**P15**.

Copolymer or complexes	E_{ox} (V)[a]	HOMO (eV)[b]	LUMO (eV)[c]	E_g (eV)	T_g[d] (°C)	T_d[e] (°C)
Ir-complex 5	0.43	5.27	2.25	3.02	na	363
Ir-complex 6	0.32	5.12	2.0	3.10	na	322
Ir-complex 7	0.30	5.10	2.0	3.10	na	300
Ir-complex 8	0.29	5.09	2.0	3.10	na	275
P1	0.98	5.78	2.84	2.94	81	410
P2	1.01	5.81	2.89	2.95	100	428
P3	1.07	5.89	2.71	3.18	130	442
P4	1.01	5.81	2.89	2.92	81	423
P5	1.03	5.83	2.89	2.94	96	430
P6	na	na	na	3.10	na	420
P7	0.91	5.71	2.76	2.95	96	420
P8	0.91	5.71	2.76	2.95	97	375
P9	1.12	5.92	2.74	3.18	na	415
P10	1.10	5.90	2.72	3.18	na	357
P11	1.02	5.82	2.64	3.18	96	360
P12	0.93	5.73	2.78	2.95	96	425
P13	0.93	5.73	2.78	2.95	98	362
P14	na	na	na	3.10	na	410
P15	na	na	na	3.10	na	365

[a] Oxidation potential is adjusted by using ferrocene ($E_{1/2}$ = 490 mV vs Ag/$AgNO_3$) as an internal reference. Conditions of cyclic voltammetruc measurements: Pt working electrode; Ag/$AgNO_3$ reference electrode. Scan rate: 100 mV/s. Electrolyte: tetrabutylammonium hexafluorophosphate. na = not detected.
[b] HOMO levels were calculated from CV potentials using ferrocene as a standard [HOMO = 4.8 + ($E_{ox} - E_{Fc}$)].
[c] LUMO levels were derived via eq. E_g = HOMO–LUMO, where E_g obtained from the absorption spectra.
[d] Obtained from DSC measurements; na = not detected.
[e] Obtained from TGA measurements. T_d values were recorded at 5% weight loss.

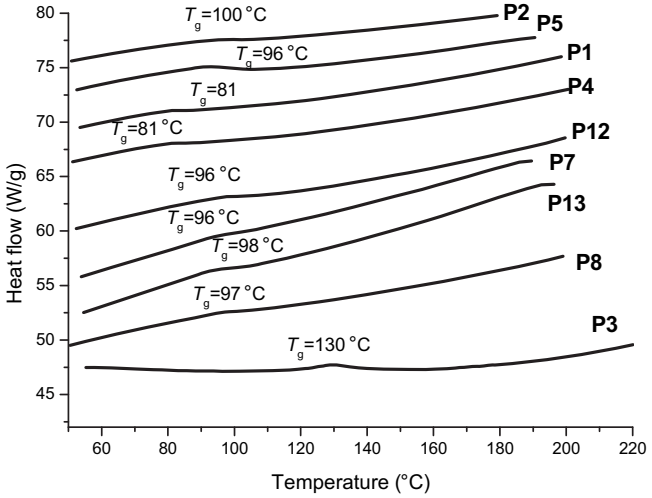

Fig. 1. DSC traces of copolymers measured under nitrogen at a heating rate of 10 °C/min.

transition temperatures (T_g) of the copolymers are in the range of 81–130 °C (see Fig. 1). Incorporation of **D** or **Do** units into the copolymer backbones results in higher T_g values than **PF** ($T_g = 75$ °C) [7b]. Such an outcome may be due to the presence of heavy atoms (sulfur) [23] and the absence of flexible hydrocarbon chains in **D** or **Do** units of the former.

3.3. Electrochemical properties

The electrochemical behavior of all Ir-complexes and Ir-copolymers were studied by cyclic voltammetric (CV) methods, and the relevant data are listed in Table 2. A reversible one-electron oxidation wave attributed to the oxidation of iridium(III) was detected at 0.43, 0.32, 0.30 and 0.29 V vs. Fc/Fc^+ for Ir-complexes **5**, **6**, **7**, and **8**, respectively. Except **P6**, **P14**, and **P15**, which showed very poor solubility in dichloromethane solutions, all Ir-copolymers showed a quasi-reversible oxidation wave with an onset potential around 0.91–1.12 V vs. Fc/Fc^+ reference electrode. The energies of the highest occupied molecular orbitals (HOMOs) in all copolymers were calculated relative to ferrocene (Fc), which had a value of 4.8 eV with respect to the vacuum level [24]. The HOMO and LUMO (lowest unoccupied molecular orbital) data are also collected in Table 2. The HOMO energies in combination with the optical band gaps (E_g) derived from the absorption band edges were used to calculate the LUMO energies of the polymers. In comparison with **PF** (HOMO = 5.77 eV; band gap = 2.76 eV) [3a], copolymers bearing **D** or **Do** units (with HOMO = 5.73–5.92 eV and band gap = 2.94–3.18 eV) have higher (or similar) HOMO energy levels and larger band gaps. There was no obvious variation of the HOMO level for copolymers upon incorporation of iridium segments, possibly due to the lower contents of the iridium units.

3.4. Optical properties

The photophysical properties of all compounds are presented in Table 3, and some selected UV–vis absorption spectra are shown in

Table 3
Photophysical properties of Ir-complexes **5–8**, copolymers (**P1–P15**), and Ir-doped copolymers (**P3** doped with 10 mol% of Ir-complexes **6** and **8**).

Compound/Copolymer	Solution					Film					
	$\lambda_{abs,max}$ (nm)[a]	$\lambda_{PL\ max}$ (nm)	Φ_f (%)	Φ_p (%)	E_T (eV)[f]	$\lambda_{abs,max}$ (nm)	$\lambda_{PL,max}$ (nm)[g]	Φ_f (%)[h]	Φ_p (%)[h]	E_T (eV)[f]	τ[i]
Ir-complex 5	303, 316, 388, 416, 450	518[b]		30[d]	2.39		539		3.6	2.30	
Ir-complex 6	340, 400, 452, 472	566[b]		25[d]	2.19		578		2.5	2.14	
Ir-complex 7	256, 304, 315, 372, 403, 430	510[b]		22[d]	2.43		523		2.3	2.37	
Ir-complex 8	295, 317, 376, 400, 428	510[b]		40[d]	2.43		520		3.3	2.38	
P1	375	418[c]	75[e]		2.25	380	439	30		2.15	0.22 ns
P2	375	416[c]	45[e]		2.25	382	426	25		2.15	0.28 ns
P3	336	384[c]	30[e]		2.39	357	410	12		2.28	0.51 ns
P4	385	418[c]	70[e]		2.24	386	440	34		2.13	0.33 ns
P5	373	417[c]	48[e]		2.26	384	440	28		2.15	0.49 ns
P6	348	415[c]	25[e]		2.36	387	428	15		2.25	0.60 ns
P7	370	418[c]	25[e]				576		2.3		0.32 μs
P8	374	418[c]	15[e]				595		1.5		0.08 μs
P9	335	384[c]	23[e]				567		4.8		0.45 μs
P10	336	400[c]	14[e]				570		3.2		0.30 μs
P11	334	387[c]	14[e]				418		0.5		0.12 μs
P12	370	422[c]	25[e]				435		3.5		0.30 μs
P13	373	424[c]	13[e]				593		2.0		0.10 μs
P14	350	420[c]	18[e]				430		5.0		0.31 μs
P15	342	425[c]	12[e]				575		3.8		0.39 μs
P3 + 3 mol% **6**							576		7.5		0.44 μs
P3 + 3 mol% **8**							410		1.8		0.12 μs
P3 + 10 mol% **6**							567		4.5		0.40 μs
P3 + 10 mol% **8**							410		1.1		0.07 μs
PVK + 3 mol% **6**							564		10.6		1.17 μs
PVK + 3 mol% **8**							568		9.7		1.04 μs
PVK + 10 mol% **6**							511		30		0.94 μs
PVK + 10 mol% **8**							515		20		1.17 μs

[a] Measured in CH_2Cl_2 solutions at 298 K.
[b] Measured in toluene solutions. Excitation wavelength was 400 nm.
[c] Measured in THF solutions. Excitation wavelength was 350 nm.
[d] The quantum yields were measured in degas toluene solutions relative to $Ir(ppy)_3$ ($\Phi_P = 0.4$ in toluene)[21]. The excitation wavelength was 400 nm.
[e] The quantum yields were measured in THF solutions in air relative to curmarin 1 ($\Phi_f = 0.99$ in ethyl acetate)[20] as a reference. The excitation wavelength was 350 nm.
[f] Measured at 77 K.
[g] The excitation was 350–400 nm.
[h] Measured with an integrating sphere under an excitation wavelength of 350 nm on a quartz glass.
[i] Measured at 298 K. The excitation wavelength was 357 nm for all copolymers. The fluorescence lifetimes and phosphorescence lifetimes were monitored at 430 and 575 nm, respectively.

Fig. 2. In Fig. 2(a), Ir-complexes **5**–**8** have strong absorption bands at 270–370 nm attributed to the π–π* transition of the benzimidazolyl ligands and relatively weaker absorption bands at 400–500 nm attributed to singlet and triplet metal-to-ligand charge-transfer [18,19], ^{1}MLCT and ^{3}MLCT. The absorption characteristics of metal-free copolymers (**P1**–**P6**) are shown in Fig. 2(b). The intense bands at 336–386 nm can be assigned to the π–π* transition of the polymer backbones. The bands shifted to shorter wavelengths as the contents of **D** (or **Do**) units increased in the polymers, indicating that the **D** (or **Do**) linkages interrupted the delocalization of π-electrons along the polymer backbones. For example, the absorption peak of **P3** was blue shifted by 39 nm compared with that of **P2** (336 nm vs. 375 nm), and the peak of **P6** was blue shifted by 25 nm compared with that of **P5** (348 nm vs. 373 nm). The absorption spectra of **P8**, **P10**, **P13** and **P15** (10 mol% iridium ratio) are shown in Fig. 2(c). Besides the π–π* transition band of the copolymer backbones and the benzimidazolyl ligands, weak absorption bands due to the ^{1}MLCT and ^{3}MLCT transitions of the iridium moieties were also noticeable in the range of ~400–500 nm [4b,7b,8b,10]. Similar to **P1**–**P6**, polymers with higher fluorene contents (**P8** and **P13**) had longer effective conjugation lengths of oligofluorene and exhibited longer absorption lengths. In comparison with the absorption spectra of **P7**, **P9**, **P12** and **P14** (3 mol% iridium ratio), the MLCT transitions were not clear and cannot be observed due to the lower ratio of iridium units.

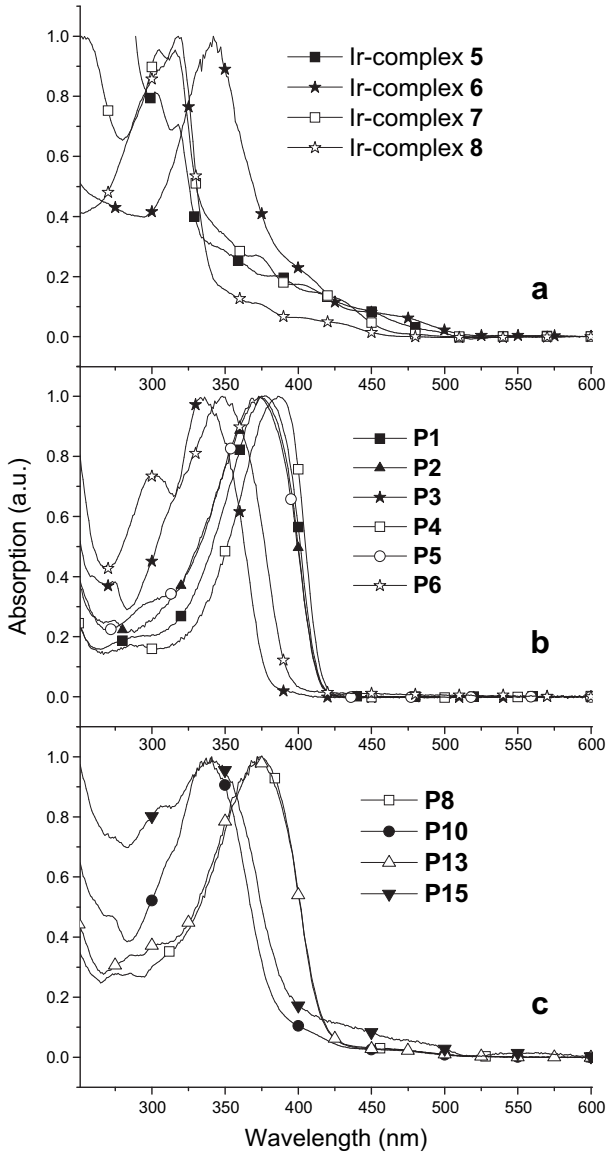

Fig. 2. UV–vis absorption spectra in CH_2Cl_2 solutions of (a) Ir-complexes **5**–**8**, (b) metal-free copolymers **P1**–**P6** and (c) selected Ir-copolymers (**P8**, **P10**, **P13** and **P15**).

The photoluminescence (PL) properties of Ir-complexes **5**–**8**, copolymers **P1**–**P15** and Ir-doped copolymer **P3** doped with 10 mol% of Ir-complexes **6** and **8** are demonstrated in Table 3. In Fig. 3(a), Ir-complexes **5**, **7** and **8** emitted in green region (λ_{max} = 510–518 nm), which were inherited from their precedent complex, **(pbi)$_2$Ir(acac)**, whose chemical structure is shown in Fig. 3(a) [18]. It is important to note that the PL emission of Ir-complex **6** emitted in the orange-yellow range (λ_{max} = 566 nm), which was attributed to the extension of the ligand conjugation with fluorene units in Ir-complex **6**. The PL spectra of selected copolymers in THF solutions and all copolymers (**P1–P15**) in solid films are shown in Fig. 3(b) and (c)–(e), respectively, while Ir-doped copolymers (**P3** doped with 3 or 10 mol% Ir-complexes **6** and **8** in solid films) are also shown in Fig. 3(f). Consistent with the absorption spectra, fluorescence wavelengths increased with increasing effective conjugation lengths (decreasing **D** or **Do** units) of the polymer both in solution and in the film state, i.e., **P1** > **P2** > **P3**, **P4** = **P5** > **P6**, **P7** > **P9** and **P12** > **P14**. Similar to **P1**–**P6**, Ir-copolymers **P7**–**P15** and Ir-doped copolymer **P3** doped with 3 or 10 mol% Ir-complexes **6** and **8** emitted only characteristic violet-blue light in dilute THF solutions due to the π–π* transition of the polymer backbones (Fig. 3(b)), indicating that energy transfer from the polymer backbones to the iridium units was very inefficient in solution. In comparison, the phosphorescence emissions of Ir-copolymers **P7**–**P15** and Ir-doped copolymers (3 and 10 mol% of iridium units) were more obvious in solid films (Fig. 3(d)–(f)), especially for the higher concentration (i.e., 10 mol%) of iridium units (see Fig. 3(e)), indicating the presence of energy transfer from the π–π* transition to MLCT bands. The efficiency of the energy transfer appeared to be higher as the **D** or **Do** ratios in the polymer backbones increased, i.e. Ir-copolymers **P9** and **P14** were more efficient than **P7** and **P12** (see Fig. 3(d)). In comparison with Ir-copolymers, Ir-doped copolymers in solid films had similar PL spectra as the corresponding analogues with equivalent concentrations of iridium units as shown in Fig. 3(f). It is important to note that the PL spectra of **P11** tethered with a green-emitting congener of **8** and Ir-doped **P3** with green-emitting Ir-complex **8** still exhibited strong blue emission from the polymer backbones in addition to the weak green emission from iridium units; that is, they had less efficient energy transfer compared to other Ir-copolymers tethered with a yellow-orange emitter (vide infra). It is believed that energy back transfer from the Ir-center to the polymer backbone also plays an important role in phosphorescence efficiency. In contrast to the long phosphorescence lifetimes of Ir-doped PVK (τ = 0.72–1.04 μs), the faster phosphorescence decay in **P7**–**P15** (τ = 0.07–0.45 μs) and Ir-doped **P3** (τ = 0.07–0.44 μs) implied that there was more facile quenching of the triplet state of the iridium complex in the latter due to triplet energy back transfers from iridium complexes to the polymer backbones. Energy back transfer was even more serious for green-emitting Ir-copolymer **P11** (τ = 0.12 μs) and Ir-doped **P3** containing 3 or 10 mol% of Ir-complex **8** (τ = 0.07–0.12 μs), which exhibited shorter phosphorescence lifetimes than PVK doped with Ir-complex **8**.

The fluorescence/phosphorescence quantum yield (Φ_f/Φ_p) values of Ir-complexes **5**–**8**, copolymers **P1**–**P15** and Ir-doped copolymer **P3** doped with 3 or 10 mol% of Ir-complexes **6** and **8** are also listed in Table 3. The Φ_p values of Ir-complexes **5**–**8** were

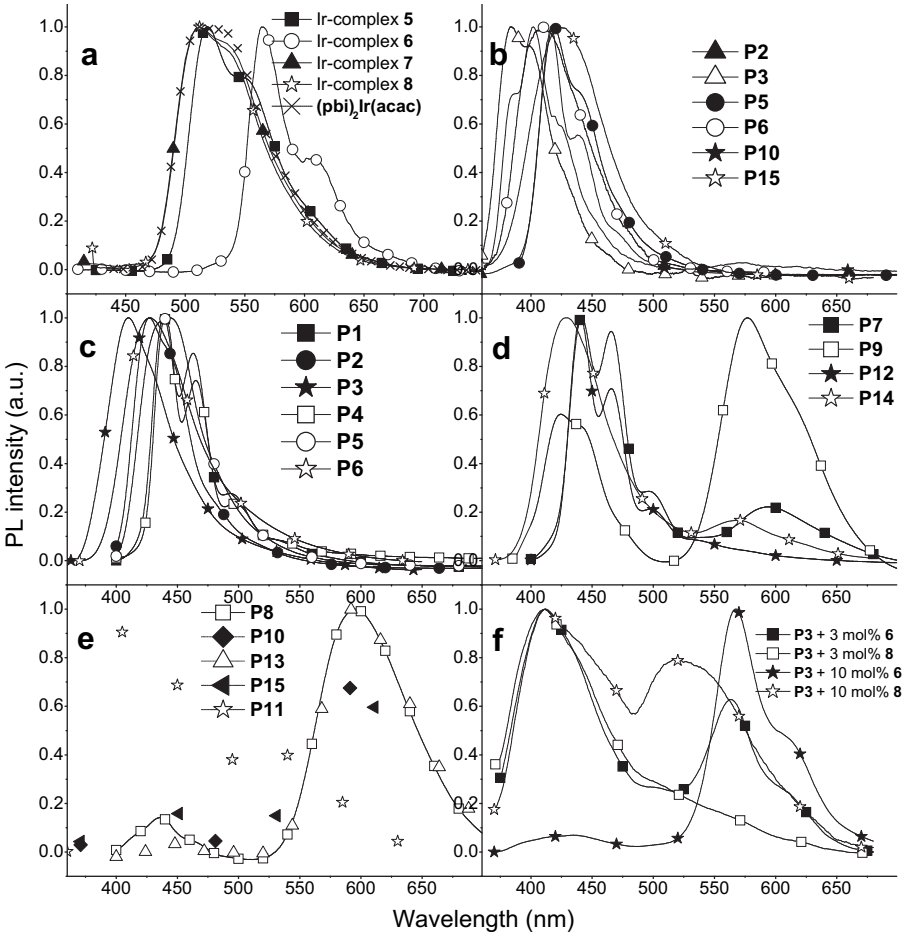

Fig. 3. PL spectra of (a) Ir-complexes **5**–**8** and **(pbi)$_2$Ir(acac)** in toluene solutions, (b) selected copolymers in THF solutions, (c) metal-free copolymers **P1**–**P6** in solid films, (d) Ir-copolymers **P7**, **P9**, **P12** and **P14** in solid films (3 mol% of iridium units), (e) Ir-copolymers **P8**, **P10**, **P11**, **P13** and **P15** in solid films (10 mol% of iridium units) and (f) selected Ir-doped copolymers in solid films.

22–40% in degassed toluene solutions and 2.3–3.6% in solid films. The Φ_f values of metal-free copolymers **P1**–**P6** ranged from 30 to 75% in THF solutions and from 12 to 34% in solid films. As the contents of **D** or **Do** units increased, the Φ_f values of **P1**–**P6** decreased in both solutions and solid films, possibly due to the presence of the heavy atom of sulfur [25]. Compared with the solid films of metal-free copolymers (Φ_f values = 12–34%), the solid films of Ir-copolymers **P7**–**P15** and Ir-doped copolymer **P3** doped with 10 mol% of Ir-complexes **6** and **8** were found to have lower Φ_p values, with ranges of 0.5–5.0% and 1.1–7.5%, respectively. In general, the PL efficiency (Φ_f and Φ_p) decreased as the contents of iridium units increased [2d,3a,3b,4b]. This can be rationalized by the greater tendency of triplet–triplet annihilation at higher iridium concentrations. However, the Φ_p values of Ir-copolymers were enhanced as the **D** (**Do**) ratio in the polymer backbone increased, i.e. **P9**, **P10**, **P14** and **P15** were higher than **P7**, **P8**, **P12** and **P13**, respectively. It is believed that the larger triplet energy (vide infra) for the polymer with higher **D** or **Do** contents (~50 mol%) can more effectively suppress the energy back transfer from the phosphor to the polymer backbone (vide infra). The quenching of phosphorescence via energy back transfer of the phosphor excited state to the polymer triplet excited state has been well demonstrated for the polymer with lower triplet energy [10].

Phosphorescence spectra of **P1**–**P6** and iridium complexes **6** and **8** in solid films were measured at 77 K (liquid nitrogen temperature) using a 5-ms delay time between the excitation with a microsecond flash lamp and the measurement. Representative phosphorescence spectra of selected copolymers (**P2**, **P3** and **P5**) are shown in Fig. 4. The triplet energies of the compounds were then determined from the peak maximum of the shortest emission wavelength in the phosphorescence spectra. The E_T values of **P1**–**P6**

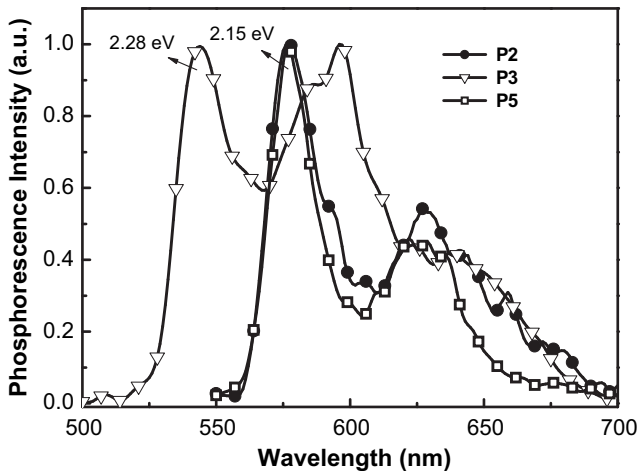

Fig. 4. Phosphorescence spectra (measured at 77 K) of some selected metal-free copolymers (**P2**, **P3** and **P5**) in solid films.

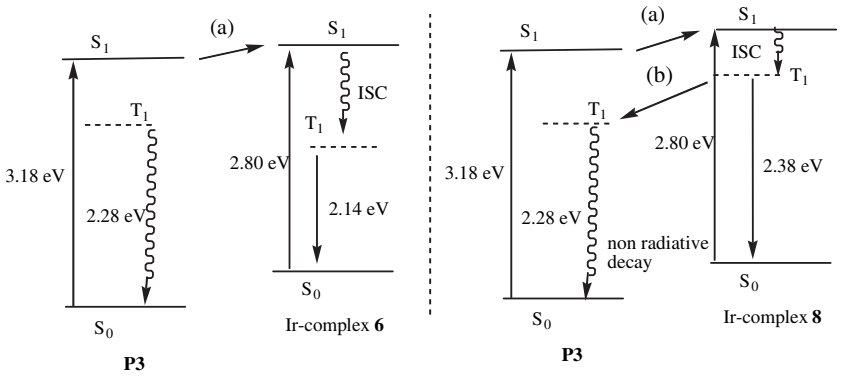

Fig. 5. Energy level diagrams (eV) of **P3** and Ir-complexes **6** and **8**.

in solid films were measured to be 2.15, 2.15, 2.28, 2.15, 2.15 and 2.25 eV, and the E_T values of Ir-complexes **6** and **8** in solid films were 2.14 and 2.38 eV (from the phosphorescent emission wavelength), respectively. The E_T increased with increasing number of **D** units, for example, **P3** > **P1** and **P2**. Illustration of relative energies of states for **P3** and Ir-complexes **6** and **8** as well as the transitions among different states are shown in Fig. 5. It is believed that the higher Φ_p values in solid films of Ir-doped copolymers (**P3** doped with 3 or 10 mol% of Ir-complexes **6** and **8**) compared with those of Ir-copolymers (**P9**–**P11**) partially benefited from the less efficient energy back transfer in the former [10]. The energy transfer efficiency depended on the distance, orientation and overlapped areas of absorption-PL spectra between the host and guest. The slightly lower PL efficiencies of Ir-copolymers may be explained by the constrained orientation of iridium complexes covalently bonded to the polymer backbones as well as the larger π–π interactions induced by the polymer main chains, which diminished the mobility of the phosphorescent iridium moieties and thus hampered the energy transfer.

3.5. Electroluminescent properties

Except for the poor solubilities of **P6**, **P14** and **P15** in chlorobenzene due to their higher **Do** contents in the polymer backbones, all copolymers can be fabricated into PLED devices by using the spin-coating technique. PLED devices were fabricated with a configuration of ITO/poly(ethylenedioxythiophene):poly(styrene–sulfonic acid) (PEDOT:PSS, 50 nm)/metal-free copolymers (**P1**–**P5**), Ir-copolymers (**P7**–**P13**) or Ir-doped copolymers (**P3** or PVK doped with 3 or 10 mol% of Ir-complexes **6** and **8**) (60–80 nm)/1,3,5-tris(*N*-phenylbenzimidazol-2-yl)benzene (TPBI) (40 nm)/LiF (1 nm)/Al (120 nm); where vacuum-deposited TPBI was used as an electron-transporting and hole-blocking layer. The configuration of PLED devices, the chemical structures of PEDOT:PSS and TPBI and the triplet energy level diagrams of the hosts and guests are all illustrated in Fig. 6. The EL spectra and the performance data of the PLED devices are shown in Fig. 7 and Table 4, respectively. The EL curves of current–voltage–brightness (*I*–*V*–*L*) characteristics along with the external quantum efficiency and power efficiency vs. current density for selected

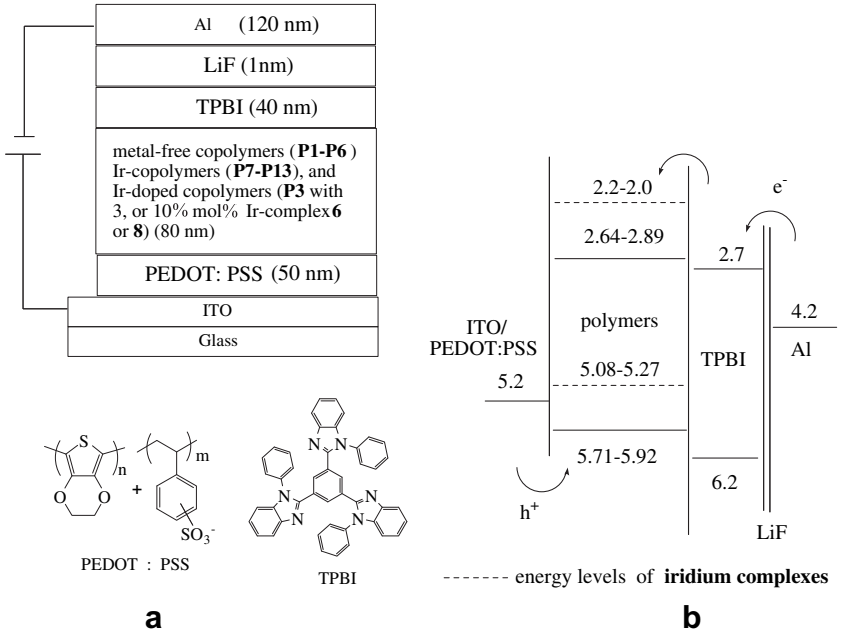

Fig. 6. (a) The configurations of PLED devices and the molecular structures of PEDOT and TPBI used in the device, and (b) the relative energy levels of the compounds utilized in the PLED devices.

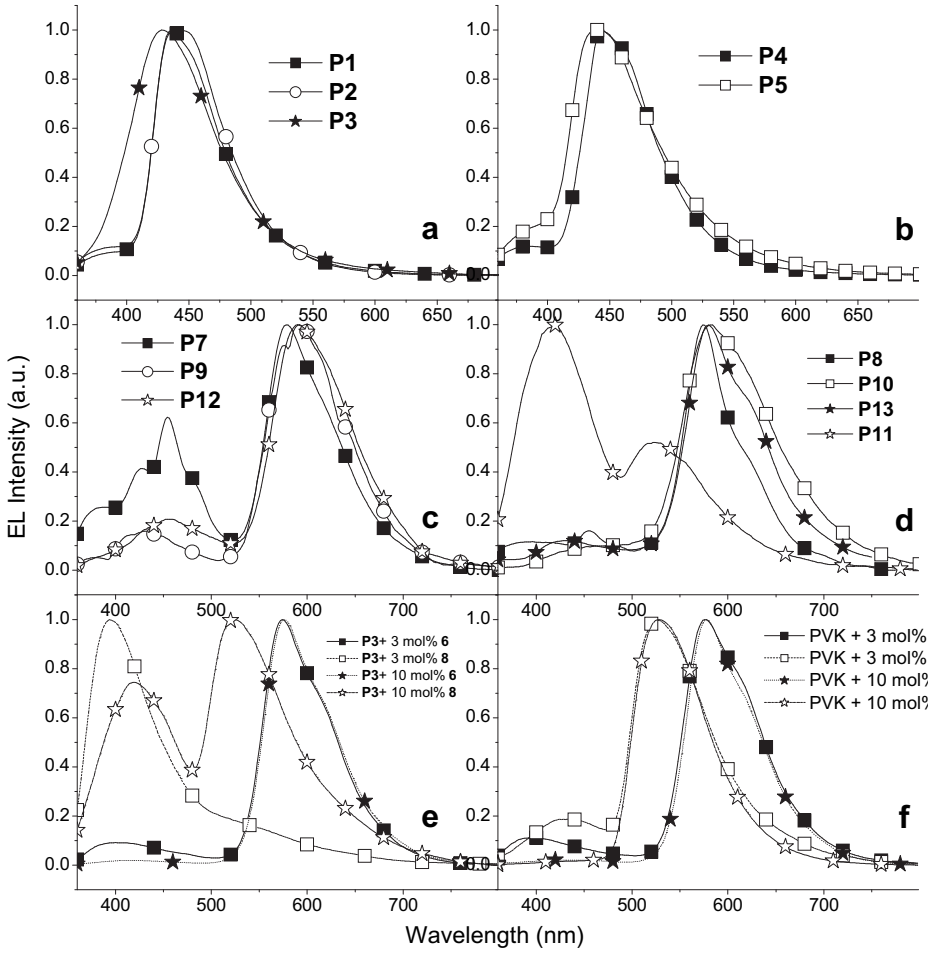

Fig. 7. EL spectra (at 9 V) of various PLED devices containing (a) and (b) metal-free copolymers, (c) Ir-copolymers (3 mol% of iridium units), (d) Ir-copolymers (10 mol% of iridium units), (e) Ir-doped copolymer **P3** with 3 or 10 mol% of Ir-complexes **6** and **8** and (f) PVK with 3 or 10 mol% of Ir-complexes **6** and **8**.

devices are shown in Figs. 8 and 9, respectively. The PLED devices without TPBI were excluded due to their extremely low efficiencies, which dropped at least one order of magnitude. Copolymer **P3** was chosen as the doped-host, because its higher E_T may increase the EL efficiencies of the PLED devices.

3.5.1. Metal-free copolymers

In Fig. 7(a) and (b), the EL spectra of metal-free copolymers **P1**–**P5** were similar to their PL spectra in solid films. The EL emission peaks of these copolymers ranged from 400 to 500 nm, which were in the deep blue region based on Commision Internationale de l'Eclarage (CIE) 1931 color coordinates. Among the metal-free copolymers (**P1**–**P5**) in Table 4, the best fluorescence PLED devices with the highest $\eta_{ext,max}$ values were found to be 1.77%, 0.71 lm/W and 1726 cd/m^2 at 14 V for **P2** and 1.53%, 0.95 lm/W and 2330 cd/m^2 at 14 V for **P5**. It is worth noting that the **P3**-based PLED device had the lowest EL efficiency in fluorescence due to its low Φ_f value in the solid film.

3.5.2. Ir-copolymers

Similar to PL spectra in solid films, the EL spectra of PLED devices from Ir-copolymers (**P7**–**P13**) shown in Fig. 7(c) and (d) had both contributions from the fluorescence of the polymer backbones and iridium moieties. However, the relative emission intensities of phosphorescence vs. fluorescence in EL spectra was higher than those in PL spectra, implying that charge trapping played an important role in the PL and EL emission colors. If the host does not have sufficiently high E_T values, energy back transfer can occur readily, which will counteract the contribution from phosphor moieties (with the maximum value of 75% theoretically). Based on the results of PL studies, the triplet energy back transfers from Ir-copolymers **P7**, **P8**, **P12** and **P13** had a greater tendency than those from Ir-copolymers **P9** and **P10**. It can be thought that copolymers with less fluorene units (e.g., **P9** and **P10** with the repeating unit of $x = 0$ and higher repeating unit of y, i.e., higher molar ratios of **D** or **Do** units) and higher iridium ratios (e.g., **P8**, **P10** and **P13** with the repeating unit of $z = 10$ and higher molar ratios of **D** or **Do** units) have higher $\eta_{ext,max}$ and $\eta_{p,max}$ values. The EL efficiencies of Ir-copolymers (**P7**–**P13**) were in the following order: **P9** ($\eta_{ext,max} = 0.90\%$, $\eta_{p,max} = 0.73$ lm/W) > **P7** ($\eta_{ext,max} = 0.80\%$, $\eta_{p,max} = 0.48$ lm/W), **P10** ($\eta_{ext,max} = 0.94\%$, $\eta_{p,max} = 0.94$ lm/W) > **P8** ($\eta_{ext,max} = 0.60\%$, $\eta_{p,max} = 0.64$ lm/W), **P10** ($\eta_{ext,max} = 0.94\%$, $\eta_{p,max} = 0.94$ lm/W) > **P11** ($\eta_{ext,max} = 0.15\%$, $\eta_{p,max} = 0.17$ lm/W), and **P13** ($\eta_{ext,max} = 0.80\%$, $\eta_{p,max} = 0.79$ lm/W) > **P12** ($\eta_{ext,max} = 0.45\%$, $\eta_{p,max} = 0.21$ lm/W). The EL efficiencies of Ir-copolymers corresponded with the Φ_p values in solid film in our observation. Being tethered with a green emitting Ir-unit possessing a higher E_T value, the **P11**-based device had much smaller $\eta_{ext,max}$ and $\eta_{p,max}$ values than **P10** tethered with a yellow-emitting unit because of the higher tendency of energy back transfer in the former. There was prominent emission from the polymer backbone in the PLED device of **P11**, as shown in Fig. 7(d).

Table 4
EL properties of PLED devices containing metal-free copolymers (**P1–P5**), Ir-copolymers (**P7–P13**), and Ir-doped copolymers (**P3** and PVK doped with 3 or 10 mol% of Ir-complexes **6** and **8**)

Polymer	V_{ON} (V)	L_{max} (cd/m^2) (at V)	$\eta_{ext,max}$ (%)	$\eta_{c,max}$ (cd/A)	$\eta_{p,max}$ (lm/W)	$\lambda_{em,max}$ (nm)	CIE (x,y)
Metal-free copolymers							
P1	6.0	1995 (14.5)	1.46	1.23	0.64	436	0.16, 0.10
P2	6.0	1726 (14.0)	1.77	1.46	0.71	440	0.15, 0.10
P3	5.5	390 (12.0)	0.85	0.62	0.23	428	0.16, 0.10
P4	5.5	694 (14.0)	0.97	0.98	0.41	444	0.15, 0.12
P5	5.0	2330 (14.0)	1.53	1.66	0.95	440	0.17, 0.14
Ir-copolymers							
P7	5.0	827 (18.0)	0.80	1.59	0.48	578	0.40, 0.33
P8	5.5	1449 (17.5)	0.60	1.42	0.64	588	0.41, 0.30
P9	6.0	1505 (13.0)	0.90	1.98	0.73	592	0.50, 0.40
P10	4.0	3517 (16.0)	0.94	2.09	0.94	584	0.50, 0.44
P11	5.0	336 (15.0)	0.15	0.44	0.17	538	0.34, 0.50
P12	5.5	499 (18.5)	0.45	0.93	0.21	590	0.49, 0.38
P13	5.0	2274 (17.0)	0.80	1.88	0.79	580	0.49, 0.42
Ir-doped copolymers							
P3 + 3 mol% **6**	4.0	2595 (19.0)	2.09	5.45	2.63	574	0.54, 0.44
P3 + 10 mol% **6**	5.0	3697 (15.0)	2.32	6.20	2.16	572	0.47, 0.43
PVK + 3 mol% **6**	4.0	3980 (14.5)	3.98	9.68	3.80	576	0.51, 0.44
PVK + 10 mol% **6**	4.5	5146 (17.0)	2.90	7.51	2.79	578	0.53, 0.45
P3 + 3 mol% **8**	4.0	149 (18.0)	0.21	0.18	0.05	394	0.21, 0.18
P3 + 10 mol% **8**	6.0	491 (17.0)	0.23	0.68	0.27	526	0.33, 0.51
PVK + 3 mol% **8**	5.0	3980 (14.5)	5.36	18.24	6.37	514	0.28, 0.61
PVK + 10 mol% **8**	5.0	3356 (18.0)	4.58	15.58	4.89	528	0.34, 0.59

V_{on}, turn-on voltage; L, luminance; V, voltage; η_{ext}, external quantum efficiency; η_c, current efficiency; η_p, power efficiency.

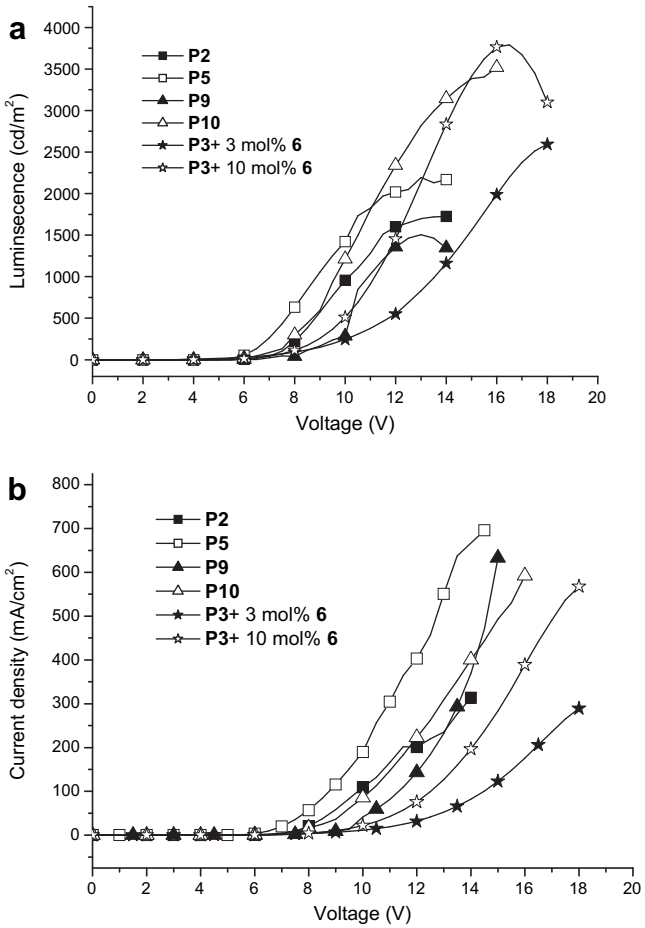

Fig. 8. The selected EL characteristic curves for PLED devices containing metal-free copolymer, Ir-copolymers and Ir-doped copolymers: (a) luminance vs. voltage and (b) current density vs. voltage.

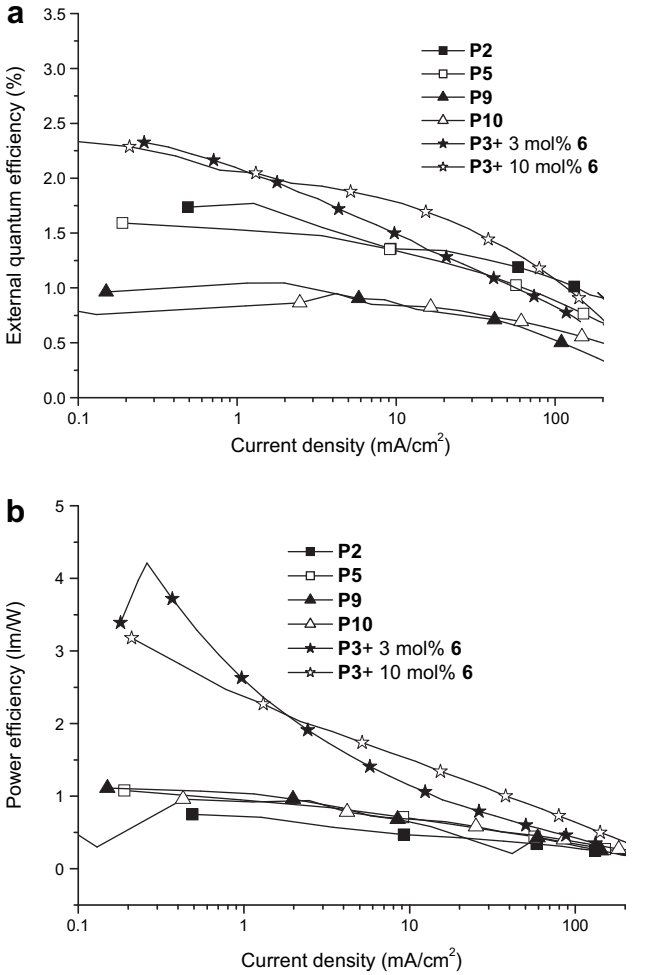

Fig. 9. The selected EL characteristic curves for PLED devices containing metal-free copolymer, Ir-copolymers and Ir-doped copolymers: (a) external quantum efficiency vs. current density and (b) power efficiency vs. current density.

3.5.3. Ir-doped copolymer

Similar to Ir-copolymers EL spectra, the EL spectra Ir-doped copolymers (**P3** or PVK doped with 3 or 10 mol% of Ir-complexes **6** and **8**) are shown in Fig. 7(e) and (f), which also had both contributions from the polymer backbones and iridium moieties. Charge trapping also played an important role here. In this study, the E_T values of **P3**, PVK and Ir-complexes **6** and **8** were 2.28, 2.50 [2a,26], 2.14 and 2.38 eV, respectively (vide supra). Therefore, the energy back transfer from Ir-complex **8** to **P3** had a greater tendency than that from Ir-complex **6** to **P3**, and the relative phosphorescence intensity of Ir-complex **8** to **P3** was smaller than that of Ir-complex **8** to PVK in the PLED devices as shown in Fig. 7(e) and (f). The trends of Ir-doped copolymers are listed as follows: (copolymer **P3** doped with 3 or 10 mol% of Ir-complexes **6** and **8**) **P3** doped with 10 mol% of Ir-complex **6** ($\eta_{ext,max} = 2.32\%$, $\eta_{p,max} = 2.16$ lm/W) > **P3** doped with 10 mol% of Ir-complex **8** ($\eta_{ext,max} = 0.23\%$, $\eta_{p,max} = 0.27$ lm/W) and **P3** doped with 3 mol% of Ir-complex **6** ($\eta_{ext,max} = 2.09\%$, $\eta_{p,max} = 2.63$ lm/W) > **P3** doped with 3 mol% of Ir-complex **8** ($\eta_{ext,max} = 0.21\%$, $\eta_{p,max} = 0.05$ lm/W). The low EL performances of **P3** doped with Ir-complex **8** (in different molar ratios, i.e., 3 and 10 mol%) can be attributed to the more facile back energy transfers from **8** to **P3**. When copolymer **P3** was replaced by PVK, the PLED performances improved significantly, especially for Ir-complex **8**-doping devices, possibly because the large triplet energy of PVK greatly suppressed the back energy transfer from Ir-complex **8**. The device efficiency of PVK doped with 10 mol% of Ir-complex **6** (2.90%, 7.51 cd/A and 2.79 lm/W) was not greatly enhanced compared to PLED of **P3** (2.32%, 6.20 cd/A and 2.16 lm/W) exhibiting the best performance. Hence, copolymer **P3** was more appropriate as the host for a yellow-orange triplet emitter than for a green triplet emitter. According to our observations, the EL efficiencies of Ir-doped copolymers also corresponded with the Φ_p values in solid film.

3.6. Hole and electron mobility properties

The space-charge limited current (SCLC) flow technique was used to measure the mobility of the charge carrier in a film [27]. The charge mobility in the hole-only or electron-only devices can be determined precisely by fitting the current vs. voltage (J–V) curve to the SCLC model for a single carrier device [28,29]. The current density is given by $J = 9\varepsilon_0\varepsilon_r\mu V^2/8L^3$ [30], where $\varepsilon_0\varepsilon_r$ is the permittivity of the polymer, $\varepsilon_0 = 8.85 \times 10^{-12}$ F/m, ε_r is the dielectric constant of the polymer, μ is the carrier mobility, and L is the film thickness. The characteristic data of the SCLC measurements are listed in Table 5.

From the capacitance–voltage measurements, the relative dielectric constants ε_r of 5.40, 6.48, 5.61, 4.32, 4.03, 10.3, 10.8, 9.22 and 7.56 were obtained for the solid films of **P2**, **P3**, **P5**, 3 mol% Ir-complex **6** + **P3**, 10 mol% Ir-complex **6** + **P3**, **P9**, **P11**, **P12** and **P13**, respectively. Therefore, their hole mobilities were calculated to be 2.10×10^{-6}, 7.67×10^{-6}, 8.51×10^{-6}, 1.91×10^{-6}, 1.58×10^{-6}, 5.38×10^{-7}, 4.42×10^{-7}, 1.34×10^{-6} and 7.05×10^{-7} $cm^2/V\,s$, respectively. The hole mobilities decreased with increasing iridium contents in the devices based on either Ir-copolymers or Ir-doped copolymers. This may be explained by the lower contents of iridium units in the system enlarging the distance between the hole-hopping sites of the polymer backbones due to the mismatch of the HOMO levels between the polymer backbones and the iridium units. Hole trapping by the iridium units might also play a role because of the higher HOMO levels of Ir-complexes **5**–**8** than those of the metal-free polymers. Possibly the presence of iridium complexes in the polymer backbones increased the spacing of hopping sites in the polymers.

Their electron mobilities were also measured and calculated to be 3.10×10^{-7}, 1.46×10^{-7}, 2.09×10^{-6}, 1.58×10^{-7}, 2.89×10^{-7}, 8.28×10^{-8}, 4.75×10^{-8}, 2.86×10^{-7} and 1.48×10^{-7} $cm^2/V\,s$, respectively. Similar to hole mobilities, the electron mobilities of iridium-containing polymers were almost one order of magnitude lower than those of metal-free polymers. The lower electron mobilities in both Ir-copolymers and Ir-doped copolymers (doped with iridium complexes) were likely due to the enlarged distance between the electron-hopping sites. In contrast to the aforementioned hole trapping, the iridium units have higher LUMO levels than the polymer backbones and were not likely to form electron traps.

In general, the electron mobilities were nearly one order lower than the hole mobilities for all copolymers. The faster hole mobilities of copolymers may cause hole decays in the cathode and inefficiency of the PLED devices. This might be the reason that the electron-transporting and hole-blocking layer, TPBI (mobility $\sim 10^{-5}$ $cm^2/V\,s$) [31], was needed for better performance of the PLED device. Though both electron and hole mobilities in Ir-doped copolymers were higher than those Ir-copolymers, (i.e. 3 mol% Ir-complex **6** in **P3** vs. **P9**), there was still an imbalance in the electron and hole mobilities in both PLED devices because the electron mobility of TPBI was ~1 or 2 orders of magnitude higher than the hole mobilities of both PLED devices. However, the insertion of a TPBI layer into the PLED devices could retard the hole mobility, which increases the probability of recombination and enhances the exciton recombination region near the interface between the emitting and TPBI layers, thus enhancing the PLED performance. The better hole and electron mobilities of metal-free copolymers and Ir-doped copolymers may improve the PLED performances.

Table 5
Characteristic data of space-charge limited current (SCLC) measurements.

Polymer	J/V^2	ε_r	L (nm)	μ ($cm^2/V\,s$)
Hole-only device				
P2	3.34	5.40	150	2.10×10^{-6}
P3	14.6	6.48	150	7.67×10^{-6}
P5	21.7	5.61	130	8.51×10^{-6}
P3 + 3 mol% **6**	2.43	4.32	150	1.91×10^{-6}
P3 + 10 mol% **6**	2.31	4.03	140	1.58×10^{-6}
P7	1.63	10.3	150	5.38×10^{-7}
P8	1.41	10.8	150	4.42×10^{-7}
P12	4.49	9.22	140	1.34×10^{-6}
P13	1.93	7.56	140	7.05×10^{-7}
Electron-only device				
P2	1.11	3.60	100	3.10×10^{-7}
P3	0.62	4.32	100	1.46×10^{-7}
P5	8.63	4.14	100	2.09×10^{-6}
P3 + 3 mol% **6**	1.26	1.73	60	1.58×10^{-7}
P3 + 10 mol% **6**	1.02	2.59	90	2.89×10^{-7}
P7	1.15	4.79	70	8.28×10^{-8}
P8	0.69	5.04	70	4.75×10^{-8}
P12	3.82	4.61	70	2.86×10^{-7}
P13	1.63	3.78	70	1.48×10^{-7}

J, electric current; V, voltage; ε_r, dielectric constant of the polymer; μ, carrier mobility; L, device thickness.

4. Conclusion

In conclusion, we have successfully synthesized a series of 2,8-disubstituted fluorene-dibenzothiophene (**PFD**) and 2,8-disubstituted fluorene-dibenzothiophene-*S*,*S*-dioxide (**PFDo**) copolymers. Copolymers with 3 and 10 mol% of covalently-bonded iridium segments in the backbones were also synthesized. The thermal stabilities of copolymers were enhanced as **D** (or **Do**) segments increased and deteriorated with increasing contents of iridium segments. Incorporation of **D** or **Do** units into the polymer backbones increased the HOMO–LUMO gaps and the triplet energy levels. As the contents of **D** or **Do** units in the copolymers increased, more efficient energy transfers were induced from the polymer

backbones to the iridium units, and less efficient energy back transfers from the iridium units to the polymer backbones occurred due to the enlarged triplet energy levels of the latter. Both Ir-copolymers and Ir-doped copolymers were used as an emitting layer of phosphorescent PLEDs. Copolymers with larger triplet energies in the polymer backbones had better performance due to more efficient suppression of energy back transfer. Less energy back transfer also led to better PLED performance for the Ir-doped copolymers compared with the Ir-copolymers. SCLC measurements carried out on both Ir-copolymers and Ir-doped copolymers confirmed that the iridium units form traps for holes and led to lower hole mobilities for both systems.

Acknowledgments

We thank the Academic Sinica, National Chiao Tung University, National Taiwan University, and National Science Council for supporting this work.

References

[1] (a) Carlise JR, Wang XY, Weck M. Macromolecules 2005;38:9000;
(b) Chen YY, Tao YT, Lin HC. Macromolecules 2006;39:8559;
(c) Chen YY, Lin HC. Polymer 2007;48:5268.
[2] (a) Gong X, Robinson MR, Ostrowski JC, Moses D, Bazan GC, Heeger AJ. Adv Mater 2002;14:581;
(b) Kawamura Y, Yanagida S, Forrest SR. J Appl Phys 2002;92:87;
(c) Lee CC, Yeh KM, Chen Y. Polymer 2008;49:4211;
(d) Jiang C, Yang W, Peng J, Xiao S, Cao Y. Adv Mater 2004;16:537;
(e) Lee CC, Yeh KM, Chen Y. Polymer 2009;50:410.
[3] (a) Zhen HY, Jiang CY, Yang W, Jiang JX, Huang F, Cao Y. Chem Eur J 2005;11:5007;
(b) Sandee AJ, Williams CK, Evans NR, Davies JE, Boothby CE, Köhler A, et al. J Am Chem Soc 2004;126:7041;
(c) Chen FC, He G, Yang Y. Appl Phys Lett 2003;82:1006;
(d) Noh YY, Lee CL, Kim JJ, Yase K. J Chem Phys 2003;118:2853.
[4] (a) Chen XW, Liao JL, Liang YM, Ahmed MO, Tseng HE, Chen SA. J Am Chem Soc 2003;125:636;
(b) Zhen H, Luo C, Yang W, Song W, Du B, Jiang J, et al. Macromolecules 2006;39:1693;
(c) Zhang Y, Xiong Y, Sun Y, Zhu X, Peng J, Cao Y. Polymer 2007;48:3468;
(d) Chen Q, Liu N, Ying L, Yang W, Wu H, Xu W. Polymer 2009;50:1430.
[5] (a) Tokito S, Suzuki M, Sato F, Kamachi M, Shirane K. Org Electron 2003;4:105;
(b) Wang XY, Prabhu RN, Schenehl RH, Weck M. Macromolecules 2006;39:3140;
(c) Li BL, Liu ZT, He YM, Pan J, Fan QH. Polymer 2008;49:1527.
[6] You Y, Kim SH, Jung HK, Park SY. Macromolecules 2006;39:349.
[7] (a) Evans NR, Devi LS, Mak CSK, Watkins SE, Pascu SI, Köhler A, et al. J Am Chem Soc 2006;128:6647;
(b) Zhang K, Chen Z, Yang C, Zou Y, Gong S, Tao Y, et al. J Mater Chem 2008;18:3366.
[8] (a) Zhang K, Chen Z, Zou Y, Yang C, Qin J, Cao Y. Organometallics 2007;26:3699;
(b) Jiang J, Jiang C, Yang W, Zhen H, Huang F, Cao Y. Macromolecules 2005;38:4072.
[9] Mei C, Ding J, Yao B, Cheng Y, Xie Z, Geng Y, et al. J Polym Sci Part A Polym Chem 2007;45:1746.
[10] Schulz GL, Chen X, Chen SA, Holdcroft S. Macromolecules 2006;39:9157.
[11] (a) Perepichka II, Perepichka IF, Bryce MR, Pålsson LO. Chem Commun 2005:3397;
(b) Dias FB, Pollock S, Hedley G, Pålsson LO, Monjman A, Perepichka II, et al. J Phys Chem B 2006;110:19329.
[12] Wang BH, Yin J, Xue MZ, Wang JL, Zhong G, Ding X. Synth Met 2003;132:191.
[13] Liu J, Zou J, Yang W, Wu H, Li H, Zhang B, et al. Chem Mater 2008;20:4499.
[14] King SM, Perepichka II, Perepichka IF, Dias FB, Bryce MR, Monkman AP. Adv Funct Mater 2009;19:586.
[15] Huang TH, Whang WT, Shen JY, Lin JT, Zheng H. J Mater Chem 2005;15:3233.
[16] Huang TH, Lin JT, Chen LY, Lin YT, Wu CC. Adv Mater 2006;18:602.
[17] (a) Niu YH, Yang W, Cao Y. Appl Phys Lett 2002;81:2884;
(b) Mikroyannidis JA, Moshopoulou HA, Anastasopoulos JA, Stylianakis MM, Fenenko L, Adachi C. J Polym Sci Part A Polym Chem 2006;44:6790.
[18] Huang WS, Lin JT, Chien CH, Tao YT, Sun SS, Wen YS. Chem Mater 2004;16:2480.
[19] (a) Huang WS, Lin JT, Lin HC. Org Electron 2008;9:557;
(b) Huang WS, Lin CW, Lin JT, Huang JH, Chu CW, Wu YH, et al. Org Electron 2009;10:594.
[20] Jones II G, Jackson WR, Choi CY, Bwrgmark WR. J Phys Chem 1985;89:294.
[21] Tsuboyama A, Iwawaki H, Furugori M, Mukaide T, Kamatani J, Igawa S, et al. J Am Chem Soc 2003;125:12971.
[22] Neumoyer CR, Amstutz ED. J Am Chem Soc 1947;69:1920.
[23] Naito K, Miura A. J Phys Chem 1993;97:6240.
[24] Pommerehne J, Vestweber H, Guss W, Mahrt RF, Bässler H, Porsch M, et al. Adv Mater 1995;7:551.
[25] Beljonne D, Cornil J, Friend RH, Janssen RAJ, Bredas JL. J Am Chem Soc 1996;118:6453.
[26] (a) Lee CL, Lee KB, Kim JJ. Appl Phys Lett 2000;77:2280;
(b) Lamansky S, Kwong RC, Nugent M, Djurovich PI, Thompson ME. Org Electron 2001;2:53;
(c) Rippen G, Kaufmann G, Klöpffer W. Chem Phys 1980;52:152.
[27] Hertel D, Bässler H. Chemphyschem 2008;9:666.
[28] Blom PWM, De Jong MJM, Van Munster MG. Phys Rev B 1997;55:R656.
[29] Dunlap DH, Parris PE, Kenkre VM. Phys Rev Lett 1996;77:542.
[30] Gill WD. J Appl Phys 1972;43:5033.
[31] Li Y, Fung MK, Xie Z, Lee ST, Hung LS, Shi J. Adv Mater 2002;14:1317.